Numerical analysis on flow and heat transfer of a tube bundle in a horizontal-tube falling film evaporator

Luopeng Yang*, Chengyong Gu, Zhexuan Xu, Xiaohong Zhang, Shengqiang Shen

School of Energy and Power Engineering, Dalian University of Technology, Dalian 116024, China, Tel. +86 131 30403891; Fax: +86 411 84707963; email: yanglp@dlut.edu.cn (L. Yang)

ABSTRACT

In order to get a better understanding of distribution characteristics of the dynamic and heat transfer performance in a horizontal-tube evaporator, a numerical calculation was developed to simulate the internal film condensation and external falling film evaporation in a tube bundle. The temperature field, film thickness and local heat transfer coefficient were predicted along the tube length and in-between tubes. In view of a good agreement of the simulated predictions with the data of the practical desalination plant, the theoretical model was proved to be valid and accurate. The results show that the flow field and heat transfer rate are improved by means of optimizing the flow density distribution of liquid film outside a tube bundle on basis of the variation of the internal condensation process. The internal vapour condensation temperature reduces sharply at the outlet of the second pass. The local overall heat transfer coefficients tend to decrease from the inlet of the tubes to the outlet and approach the maximum at the bottom of the bundle.

Keywords: Condensation; Evaporation; Temperature field; Film thickness; Tube bundle

1. Introduction

Due to the increase in population, economic activities and pollution, many countries are suffering from serious water shortages. The industrial desalination of seawater has proved to be a viable way to provide sustainable sources of fresh water. Currently available technologies for commercial desalination plants include multi-stage flash, low-temperature multi-effect distillation (LT-MED) and reverse osmosis. As LT-MED has some technical advantages through the high efficient falling film evaporation, the possibility of utilizing waste heat sources and reducing scaling and corrosion problems, it becomes the dominant thermal desalination process.

LT-MED attracts significant experimental concerns. A diverged performance along the tube bundle depth was observed. The heat transfer coefficients for plain surfaces were found to increase from row to row in a square-pitch arrangement [1–5] while a decrease in heat transfer coefficients from row to row in a triangular-pitch arrangement was obtained [6,7]. The effects of maldistribution and partial dryout on heat transfer coefficients of tube bundle were experimentally

*Corresponding author.

investigated. Compared with the upper tubes, the heat transfer coefficients for the lower tubes obviously decreased due to the occurrence of partial dryout on the surface [3]. For all wetting surface, the upper tubes exhibit a higher performance as a result of the impact of liquid from the feeder [8–10]. The effects of the structure and flow parameters on the bundle-averaged heat transfer coefficients were measured. For the wetting surface condition, an increase in flow rate reduced the bundle averaged because of increasing film thickness [1]. When dry patches appeared, a flow rate increase was more likely to increase the bundle average due to the decreasing dryout [3,6,10,11]. The behaviour of heat transfer coefficients with increasing heat flux was closely related with the flow regimes on the surface. The heat transfer coefficient decreased as the dry area increased [2,3,11]. Under the dominance of boiling effect, the heat transfer coefficient increased [2,5,6,9,12]. The heat transfer coefficient was kept almost constant for convective conditions.

Although the preceding experimental research served to provide a fundamental understanding of the falling film evaporation on a horizontal-tube bundle, few efforts made an attempt to predict the distribution characteristics of the dynamic and heat transfer performance in a horizontal-tube evaporator due to the complex three-dimensional flow condition in the evaporator. The complicated flow condition, together with the complex configuration of the tube bundle, makes it almost impossible to precisely observe and measure the comprehensive flow dynamic and heat transfer data. The absence of the true information on the flow and heat transfer of a tube bundle confines the demand to improve the tube bundle configuration and optimize the operating parameters.

In order to get a better understanding of distribution characteristics of the dynamic and heat transfer performance in a horizontal-tube evaporator,

a numerical model was developed to simulate the internal film condensation and external falling film evaporation in a tube bundle. The local temperature field, film thickness and heat transfer coefficient of both the internal condensation and external evaporation were predicted along the tube length and in-between tubes. The detailed description of the thermal performance in the tube bundle contributes to acquaint the flow and heat transfer phenomena in a horizontal-tube falling-film evaporator.

2. Mathematical models

The coordinate system for film evaporation inside a horizontal tube is shown in Fig. 1. The steady-state differential equations for the condensate film flow are given:

Continuity equation:

$$\frac{\partial u}{\partial x} + \frac{\partial v}{\partial y} + \frac{\partial w}{\partial z} = 0 \tag{1}$$

X momentum equation:

$$\frac{\partial^2 u}{\partial y^2} = -\frac{(\rho_1 - \rho_v)}{\mu_l} g \sin\theta \tag{2}$$

Z momentum equation:

$$\frac{\partial^2 w}{\partial y^2} = \frac{1}{\mu_l}\frac{dp}{dz} \tag{3}$$

Energy equation:

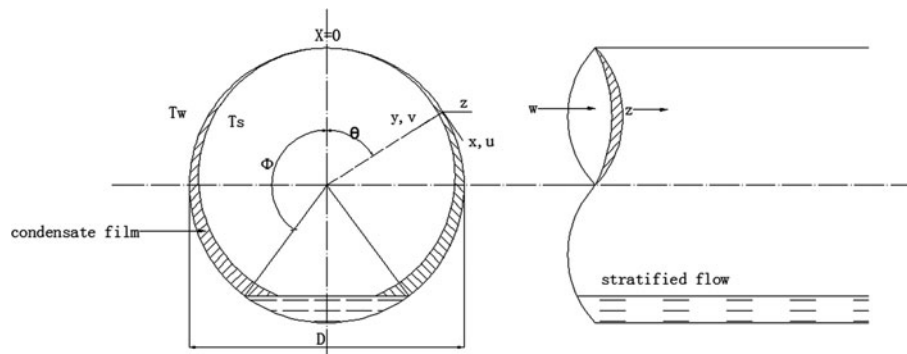$$\frac{\partial^2 T}{\partial y^2} = 0 \tag{4}$$

Fig. 1. Schematic of film condensation inside a horizontal tube.

Interfacial mass balance equation:

$$m_l = \rho_l \left(v - u\frac{\partial \delta}{\partial x} - w\frac{\partial \delta}{\partial z} \right)_{y=\delta} \tag{5}$$

Interfacial energy balance equations:

$$m_l h_{fg} = -k_l \left(\frac{\partial T_l}{\partial y} \right)_i \tag{6}$$

$$\left(u\frac{\partial \delta}{\partial x} + w\frac{\partial \delta}{\partial z} - v \right)_{y=\delta} = \left(\frac{k_l}{h_{fg}\rho_l}\frac{\partial T}{\partial y} \right)_{y=\delta} \tag{7}$$

The x velocity u, z velocity w and temperature T are givens as

$$u = g(\rho_l - \rho_v)(\delta y - 0.5y^2)\sin\theta / \mu_l \tag{8}$$

$$w = \frac{c_1}{2}y^2 + \left(\frac{\tau_i}{\mu_l} - \frac{1}{\mu_l}\frac{dp}{dz}\delta \right)y \tag{9}$$

$$T = T_w + (T_S + T_W)y/\delta \tag{10}$$

The boundary conditions of film velocity and temperature are

$$u = w = 0 \quad T = T_W \quad \text{at } y = 0 \tag{11}$$

$$T = T_S \quad \text{at } y = \delta \tag{12}$$

The equation for u, w, T and interfacial energy balance equation are substituted into continuity equation,

thus a partial differential equation for film thickness is given as

$$\frac{\partial}{\partial x}\left[\frac{g(\rho_l - \rho_v)}{3\mu_l}\delta^3 \sin\theta \right]$$
$$+ \frac{\partial}{\partial z}\left[\frac{1}{\mu_l}\frac{dp}{dz}\frac{\delta^3}{6} + \left(\frac{\tau_i}{\mu_l} - \frac{1}{\mu_l}\frac{dp}{dz}\delta \right)\frac{\delta^2}{2} \right] \tag{13}$$
$$= \frac{k_l}{h_{fg}\rho_l}\frac{(T_S - T_W)}{\delta}$$

The models of film thickness, film velocity, film temperature and local heat transfer coefficient for external falling film evaporation are developed by applying the continuity, momentum and energy equations [13].

3. Results and discussion

A LT-MED includes several consecutive effects maintained at decreasing evaporating temperature from the first effect to the last one shown in Fig. 2. Each effect is fitted with a horizontal tubes bundle. Heating vapour is introduced into the tubes of the first pass, where most parts condense into distillation. The rest completely condenses in the second pass. Simultaneously, feed seawater sprays on the tubes bundle and forms falling film on the outside the tubes by gravity. The falling film warms up to its saturated temperature on the upper tube rows of the second pass, then partly evaporates by recovering the latent heat on the lower tube rows. The produced vapour serves as a heating medium for the next effect where the processes of falling film evaporation and internal condensation repeat.
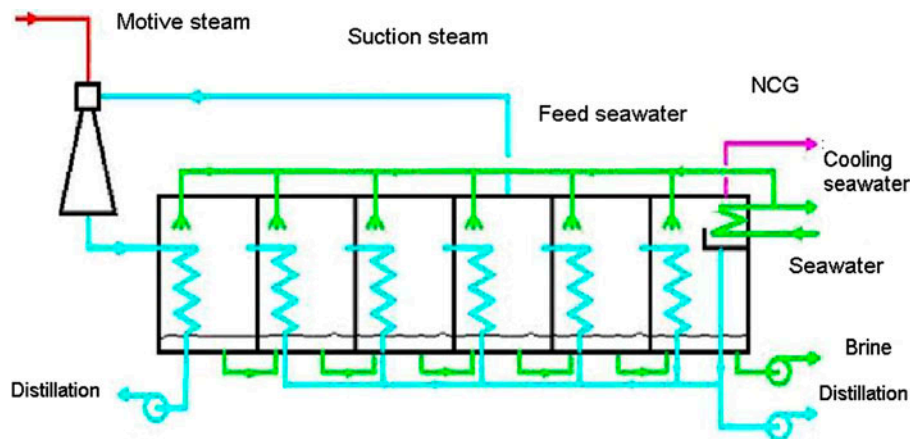

Fig. 2. Schematic of LT-MED.

Shown in Fig. 3 and Table 1 is a comparison of the evaporation temperature and water production rate in effect between the numerical prediction and the practical data of a reference LT-MED desalination plant with a capacity of 1,200 t/d. The configuration of the LT-MED with six effects of evaporators is presented in Fig. 2. The results show that the numerical prediction agrees well with the practical data within the maximum discrepancy of 7%. This good agreement proves that the simulation models are accurate and reliable. An overestimate of evaporation temperature and
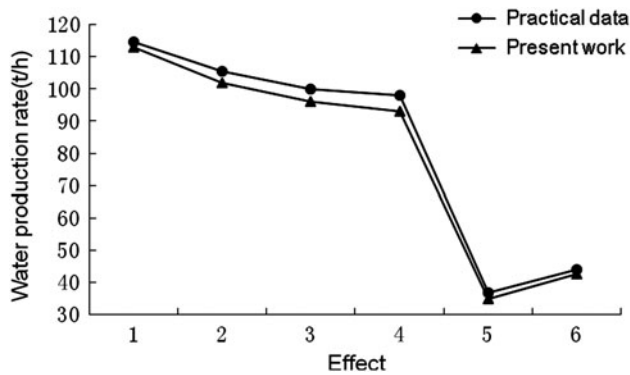
water production rate in effect is observed to grow from the first effect of the evaporator to the last. The discrepancy may be attributed to the negative effect of non-condensable gas accumulation on the internal condensation, which is not taken into account in this simulation model.

Fig. 4 presents a plot of local film thickness as a function of the tube length and vertical tube row for even distribution of seawater nozzles. The local film thickness keeps almost constant for the tubes of the second pass when the tube row number, $N < 12$. For the first pass, when $N \geq 12$, it reduces from the upper tubes to the bottom ones and increases along the tube length. This is due to the fact that the subcooling seawater does not evaporate until it preheats to its saturated temperature in the second pass, and that falling film evaporation takes place in the first pass. The uneven distribution of film thickness, which is caused by a decrease in heat transfer coefficients of internal condensation from the tube inlet to the outlet, does not favour the overall heat transfer efficiency.

Instead of the even distribution of seawater spray nozzles, an uneven distribution of seawater spray nozzles, which are distributed linearly to the heat transfer rate, is utilized. Therefore, the film thickness stays constant along the tube length in the first pass, which attributes to avoiding dry patch at the outlet of the bottom tube. A comparison of the local heat transfer coefficient of falling film evaporation between the even and uneven distributions, shown in Fig. 5, demonstrates that the heat transfer rate of the latter is enhanced.

Fig. 6 shows the temperature fields of the tube bundle for the external seawater film and the internal vapour condensation. The subcooling seawater film temperature increases smoothly to its saturated

Fig. 3. Comparison of water production rate.

Table 1
Comparison of evaporation temperatures

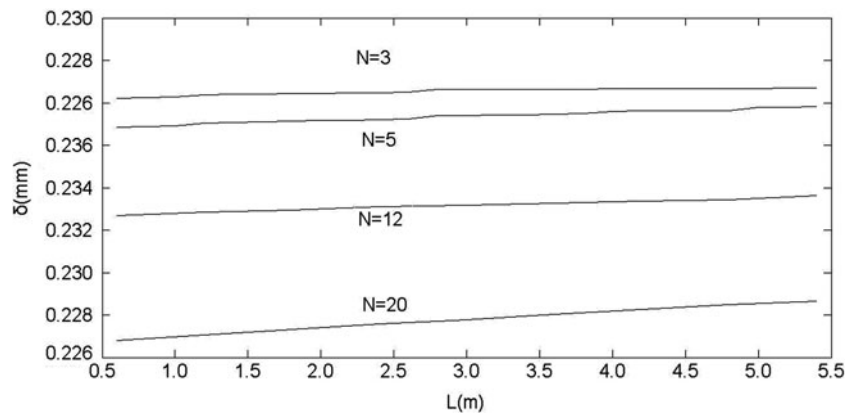| Evaporation temperatures (℃)	Effect 1	Effect 2	Effect 3	Effect 4	Effect 5	Effect 6
Present work	61.59	58.40	55.28	52.28	49.26	46.06
Practical values	61.6	58.4	55.2	52.1	49.1	45.8

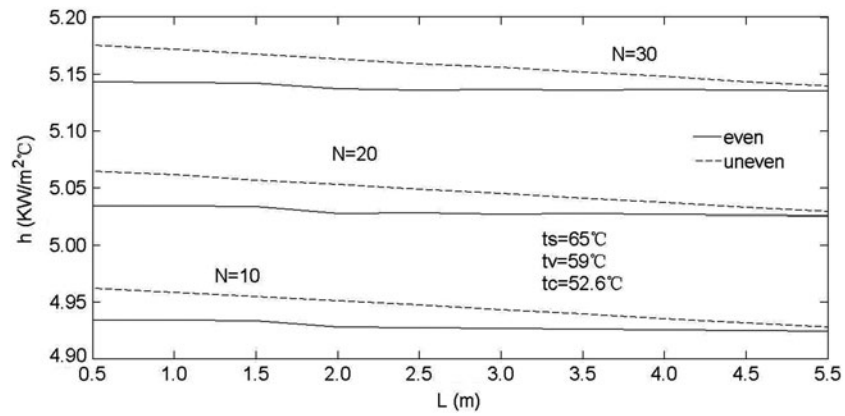Fig. 4. Local film thickness for the tube bundle.

Fig. 5. Comparison of local heat transfer coefficients for even and uneven distributions.
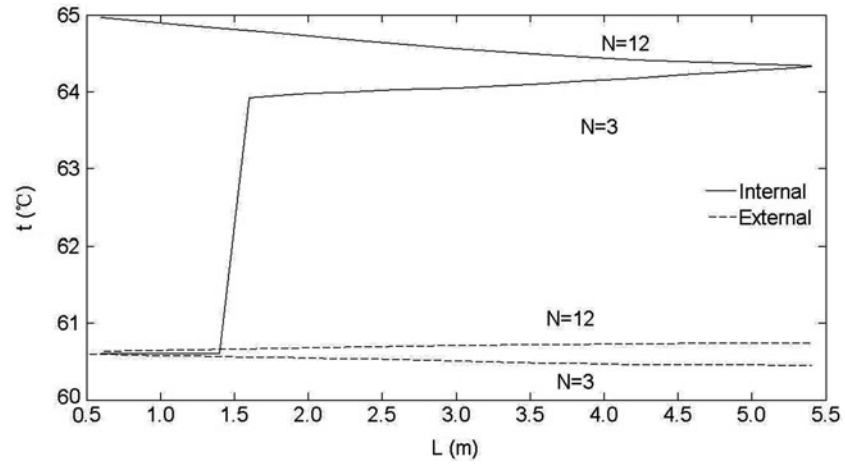

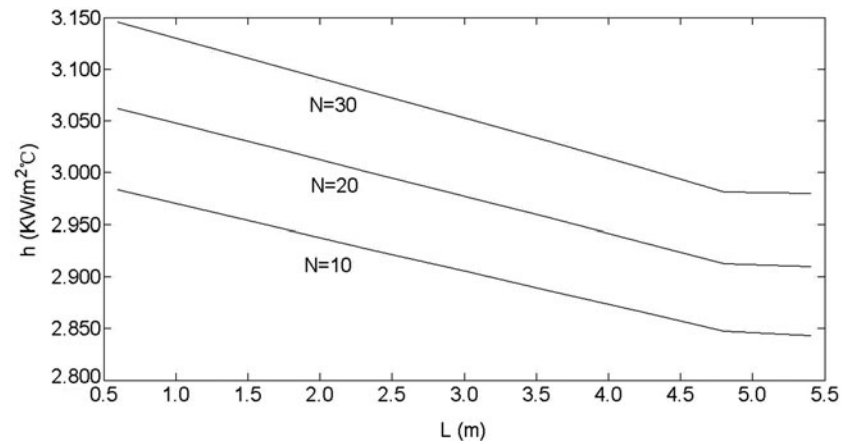Fig. 6. Temperature fields of external film and internal condensation.

Fig. 7. Profile of overall heat transfer coefficients in the tube bundle.

temperature in the second pass when $N < 12$. It is also shown that internal vapour condensation temperature reduces sharply at the outlet in the second pass when N=3. The inadequate utilization of the heat transfer area lies in the fact that almost all the internal vapour completely condenses at the outlet. Reducing the subcooling temperature difference by preheating the feed seawater contributes to improve the heat transfer efficiency.

Fig. 7 shows the profile of overall heat transfer coefficients of the tubes bundle. A decreasing overall heat transfer coefficients along the tube length is caused by the facts that the internal condensate film around the circumference of the tubes tends to increase along the tube length, and that the increase in the accumulated condensate layer at the tube bottom reduces the effective heat transfer area. The decrease in overall heat transfer coefficients and effective heat transfer area, together with the reducing thermal driving force caused by the friction between vapour and condensate inside the tubes, significantly depresses the heat transfer efficiency at the outlet, which proves the necessity of the two-pass tubes bundle.

4. Conclusions

A simulation was presented to solve the distribution characteristics of the dynamic and heat transfer performance of the tube bundle.

A satisfactory agreement of the predictions with the practical data of a reference LT-MED desalination plant proves that the developed model is accurate and reliable.

The optimizing flow density of liquid film outside a tube bundle, which is distributed linearly to the internal condensation heat transfer rate along the tube length, enhances the falling film evaporation process.

A comprehensive investigation on falling film thickness, temperature field and heat transfer coefficients describes the complex flow and characteristics of heat transfer performance in a horizontal-tube evaporator, which contributes to understand the mechanics of the tubes bundle.

Acknowledgement

Nomenclature

D	—	diameter of tube m
g	—	acceleration of gravity N/m^2
h_{fg}	—	latent heat W/(m^2 ℃)
k	—	thermal conductivity W/(m^2 ℃)
m	—	quality kg
T	—	temperature K
u	—	tangential velocity m/s
v	—	radial velocity m/s
w	—	axial velocity m/s
x	—	tangential
y	—	radial
z	—	axial
δ	—	film thickness m
ρ	—	density kg/m^3
θ	—	inclination angle, measured from the top of horizontal tube degree°
μ	—	dynamic viscosity N s/m^2
Φ	—	angular position of liquid at the bottom of tube°

Subscripts

l	—	liquid phase
S	—	saturated vapour
v	—	vapour phase
W	—	tube wall

References

[1] S.A. Moeykens, B.J. Newton, M.B. Pate, Effects of surface enhancement film-feed supply rate, and bundle geometry on spray evaporation heat transfer performance, ASHRAE Trans 101(2) (1995) 408–419.

[2] S.A. Moeykens, J.E. Kelly, M.B. Pate, Spray evaporation heat transfer performance of R-123 in tube bundles, ASHRAE Trans. 102(2) (1996) 259–272.

[3] Y. Fujita, M. Tsutsui, Experimental investigation of falling film evaporation on horizontal tubes, Heat Transfer Jpn. Res. 27 (1998) 609–618.

[4] Z.H. Liu, Q.Z. Zhu, Y.M. Chen, Evaporation heat transfer of falling film on a horizontal tube bundle, Heat Transfer Asian Res. 3 (2002) 42–55.

[5] G.N. Danilova, V.G. Burkin, V.A. Dyundin, Heat transfer in spray-type refrigerator evaporators, Heat Transfer Soviet Res. 8 (1976) 105–113.

[6] J.J. Lorenz, D. Yung, Film breakdown and bundle-depth effects in horizontal-tube, falling-film evaporators, J. Heat Transfer 104 (1982) 569–571.

[7] S.A. Moeykens, M.B. Pate, Effect of lubricant on spray evaporation heat transfer performance of R-134a and R-22 in tube bundles, ASHRAE Trans. 102(1) (1996) 10–426.

[8] M.-C. Chyu, X. Zeng, Z.H. Ayub, Nozzle-spray flow rate distribution on a horizontal tube bundle, ASHRAE Trans. 101(2) (1995) 443–453.

[9] X. Zeng, M.-C. Chyu, Z.H. Ayub, Performance of nozzle-sprayed ammonia evaporator with square-pitch plain-tube bundle, ASHRAE Trans. 103(2) (1997) 68–81.

[10] R. Armbruster, J. Mitrovic, Heat transfer in falling film on a horizontal tube, Proc. Nat. Heat Transfer Conf. Portland ASME HTD 12 (1995) 13–21.

[11] T.B. Chang, J.S. Chiou, Spray evaporation of R-141b on a horizontal tube bundle, Int. J. Heat Mass Transfer 42 (1999) 1467–1478.

[12] X. Zeng, M.-C. Chyu, Z.H. Ayub, Experimental investigation on ammonia spray evaporators with triangular-pitch plain tube bundle, Part II: Evaporator performance, Int. J. Heat Mass Transfer 44 (2001) 2081–2092.

[13] L.P. Yang, Z.X. Xu, Characterization of the microscopic mechanics in falling film evaporation outside a horizontal tube, Desalination for the Environment, Clean Water and Energy, Limassol, Cyprus, May 11–15, 2014.